NJC

PAPER

View Article Online
View Journal | View Issue

Cite this: *New J. Chem.*, 2017, **41**, 5802

Aza boron-pyridyl-isoindoline analogues: synthesis and photophysical properties†

Hui Zhang,‡[a] Yanping Wu,‡[b] Minhui Fan,[a] Xuqiong Xiao,[b] John Mack, *[c] Gugu Kubheka,[c] Tebello Nyokong [c] and Hua Lu *[b]

Received 1st March 2017,
Accepted 30th May 2017

DOI: 10.1039/c7nj00707h

rsc.li/njc

Several aza boron-pyridyl-isoindoline analogues are synthesized through a facile and scale-up two step reaction using 1,2-naphthalenedicarbonitrile as a starting material. These analogues show broad envelopes of intense vibrational bands in the absorption spectra with moderate fluorescence quantum yields in solution and the solid-state. An analysis of the structure–property relationships is described based on X-ray crystallography, optical spectroscopy, and theoretical calculations.

Introduction

In recent years there has been multidisciplinary interest in novel organic fluorescent dyes, due to their potential applications in various fields, such as organic electronics and photonics, bioimaging, and photodynamic therapy.[1] Boron dipyrromethenes (BODIPYs) have emerged as one of the most important types of chromophores in this regard.[2] In recent years, considerable effort has been devoted to preparing novel types of emissive BF_2-coordinated dyes that can be used in new applications.[3] Compared with the conventional BODIPY system, which has a straightforward synthesis based on pyrrole heterocycles, a facile and widely used preparation of asymmetric BF_2-coordinated dye is still a challenge.[2]

Recently, our group developed a facile and large-scale synthetic method to form rigid asymmetric BF_2-coordinated dyes. The oxo-pyridyliminoisoindoline precursor can be prepared in high yield by heating equivalent amounts of an imino-derivative of an isoindoline and an aminopyridine, and the precursor can then coordinated by BF_2.[4,5] This approach offers many advantages: (1) readily available, cheap and diverse starting materials; (2) facile synthesis with moderate to high total yields; (3) a large range of possible rigid target dye structures; (4) the formation of dyes with large Stokes shifts; and (5) dyes that exhibit strong fluorescence both in solution and solid-state.[5] Herein, we develop the initial study further by reporting the synthesis and properties of several aza boron pyridyl-isoindoline analogues (**1–4**) in which the position of benzo-fusion on the pyridyl moiety is changed, since this has been shown to have a significant effect in the context of BODIPY dyes.

Results and discussion

Four aza boron-pyridyl-isoindoline analogues were synthesized by heating equivalent amounts of an 3-imino-1,2-benzoisoindoline-1-one with either amino-pyridine or an amino-(iso)quinoline, followed by coordination with BF_2 (Scheme 1).[4] These dyes were characterized by high resolution mass spectrometry and ^{1}H NMR spectroscopy. The structures were further confirmed by a single crystal X-ray analysis of **1**. According to the reaction mechanism, two isomers labelled **a** and **b** should be formed when 1,2-naphthalenedicarbonitrile reacts with *N*,*N*-diethyl-hydroxyl-amine in freshly distilled dry $CHCl_3$.[6] Unexpectedly, isomer **a** was not found and **d** (1*H*-benzo[*e*]isoindole-1,3(2*H*)-dione) was isolated instead. The structure of **d** was confirmed

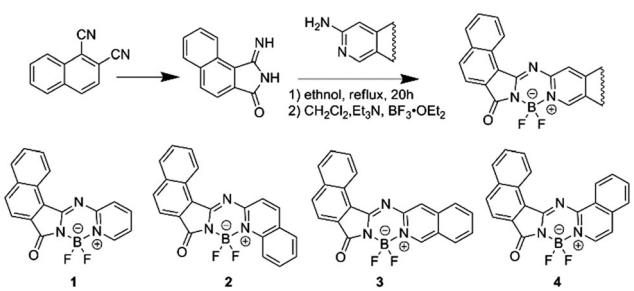

Scheme 1 Synthesis and chemical structures of **1–4**.

[a] *College of Biology and Environmental Engineering, Zhejiang Shuren University, Hangzhou, 310015, P. R. China*
[b] *Key Laboratory of Organosilicon Chemistry and Material Technology, Ministry of Education, Hangzhou Normal University, Hangzhou, 310012, P. R. China. E-mail: hualu@hznu.edu.cn*
[c] *Department of Chemistry, Rhodes University, Grahamstown 6139, South Africa. E-mail: j.mack@ru.ac.za*

† Electronic supplementary information (ESI) available. CCDC 1503936 for **1** and 1503937 for **d**. For ESI and crystallographic data in CIF or other electronic format see DOI: 10.1039/c7nj00707h

‡ These authors contributed equally to this work.

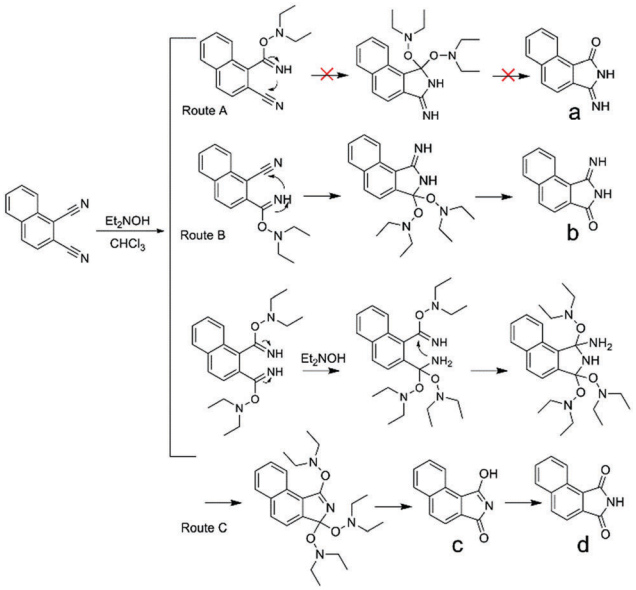

Scheme 2 Plausible reaction mechanisms for the formation of isomers **b** and **d**.

by X-ray single crystal analysis (Fig. S1, ESI†). A plausible reaction mechanism for its formation is shown as route C in Scheme 2. The most likely explanation is that steric hindrance between one of the two *N*,*N*-diethyl groups and the fused benzo ring at the isoindoline unit means that route A is disfavoured.

Suitable crystals of **1** were obtained for X-ray analysis by slow diffusion of hexane into their dichloromethane solutions. The B1–N1 (pyridine nitrogen) bond distance of **1** (1.598 Å) is about 0.09 Å longer than the B1–N2 (isoindoline nitrogen) bond distance (1.504 Å) due to the asymmetry of the structure. Similar to the previously reported structure,[4] **1** exhibits similar planar structures with average root-mean-square deviations of 0.0943 Å (Fig. 1). The boron atom of **1** has a tetrahedral geometry and the plane defined by F–B–F atoms is perpendicular to the plane of the core structure. The molecule shows partially overlapping π–π stacking and multiple short hydrogen bonding interactions within the crystals: F1···H13–C13 (2.48 Å), F2···H7–C7 (2.52 Å), O1···H8–C8 (2.41 Å), O1···H15–C15 (2.56 Å) (Fig. 2).

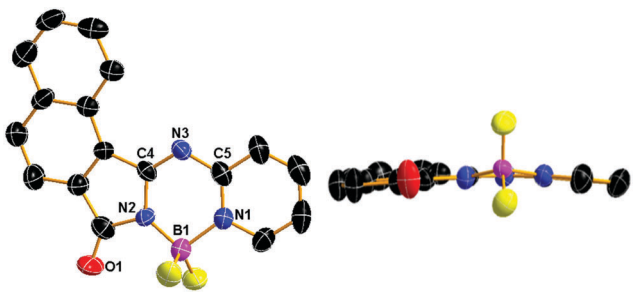

Fig. 1 Front (left) and side (right) views of the molecular structures of **1** with the thermal ellipsoids set at 50% probability. Hydrogen atoms are omitted for clarity. Selected bond lengths [Å], for **1**: B1–N2 1.504(5), B1–N1 1.598(8), N3–C4 1.293 (8), N3–C5 1.396 (3).

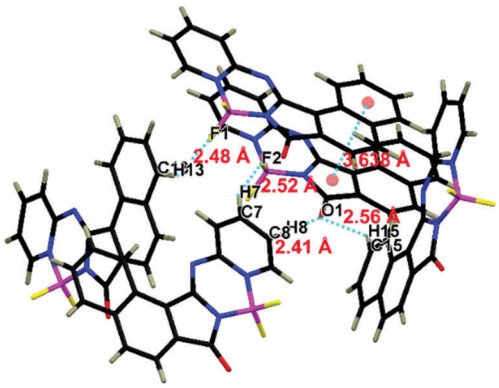

Fig. 2 View of C–H···F, C–H···O and π···π interactions of **1**.

The photophysical properties of **1–4** were analyzed in dichloromethane. These compounds have relatively broad absorption and emission bands as shown in Fig. 3, since there is considerable vibronic intensity in contrast with the narrow intense bands that are observed for conventional BODIPY dyes. The absorption spectrum of **1** contains an intense peak at 378 nm with a weaker shoulder at 396 nm. Upon benzo-fused at the 2,3-positions of the pyridyl ring to form **2**, the main band red shifts to 402 nm with a shoulder of absorbance at 423 nm. Benzo-fusion at the 3,4- and 4,5-positions to form **3** and **4** have major absorption peaks at 407 and 430 nm, respectively, and shoulder peaks at 415 and 437 nm.

In contrast with aza-BODIPYs, which retains the narrow intense emission bands of conventional BODIPY dyes,[2d,7] the emission spectra of **1**, **2** and **4** have relatively broad bands at

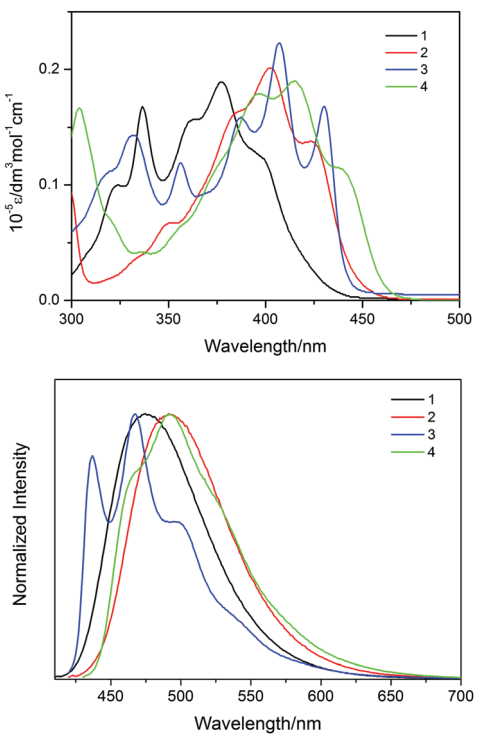

Fig. 3 Absorption (top) and emission (bottom) spectra of **1–4** (10^{-5} M) in CH_2Cl_2.

475, 492 and 492 nm, respectively, with a shoulder at 470 nm in the spectrum of **4** (Fig. 3). In contrast, narrower bands are observed in the spectrum of **3** at 437 and 467 nm. When the Stokes shift values are compared with those of classical BODIPY dyes,[2d,7] it becomes clear that the values **1**, **2** and **4**, which lie in the 2500–4200 cm^{-1} range, are much larger than the relatively small values that have been reported for symmetric dipyrromethene structures.[2] It is noteworthy, however, that a much smaller value is observed for the 3,4-position fused **3** compound, since the main electronic bands are well resolved (Fig. 3). Moderate emission intensity is consistently observed with fluorescence quantum yields of 0.24 (**1**), 0.25 (**2**), 0.21 (**3**), and 0.39 (**4**). The fluorescence lifetimes of 4.14 ns for **1**, 4.19 ns for **2**, and 1.93 ns for **3**, 2.52 ns for **4**, are consistent with what is normally observed with organic dyes with planar π-conjugation systems.[2]

The emission bands of **1–4** in the solid state are red shifted by *ca.* 10–35 nm relative to the bands in solution and are broader in shape (Fig. 4 and Table 1), the shoulder band of **2–4** in the long wavelength region are also observed. This can be attributed to the intermolecular interactions and inhomogeneous broadening. **1–4** display weak solid-state emission with fluorescence quantum yields of 0.12 for **1**, 0.06 for **2**, and 0.10 for **3**, 0.05 for **4**, respectively. The introduction of the fused benzene ring on the pyridyl moiety leads to a decrease in the fluorescence quantum yields in the solid state.

The observed trends in the electronic absorption spectra can be readily rationalized through a comparison with the trends predicted in theoretical calculations for the energies of the frontier π-MOs (Fig. 5) and the energies of the observed spectral bands in TD-DFT calculations (Fig. 6) for **1–4** and model compounds (Scheme 3). The introduction of the sp^2 hybridized oxygen atom at the 3-position and a pyridine ring into the structure of aza-BODIPY results in a stabilization of the HOMO and a destabilization of the LUMO due to the introduction of extra angular nodal planes (Fig. 7) and hence there is a markedly greater HOMO–LUMO gap (Fig. 5) and blue shift of the main spectral band (Fig. 6). When a naphthalene group is fused to the β-carbons of the pyrrole ring, extra π-MOs are introduced so that the MO derived from the HOMO of aza-BODIPY is no longer the HOMO of **1–4** (Fig. 5). This accounts for the weaker shoulder bands that observed to the red of the main in the spectra of **1**, **2** and **4** at 396, 423 and 437 nm (Fig. 3), while the more intense bands at 378, 402 and 415 nm can be assigned to the transitions between the MOs derived from the HOMO and LUMO of aza-BODIPY, which is the HOMO−1 in the context of **1–4** (Fig. 5 and 7).

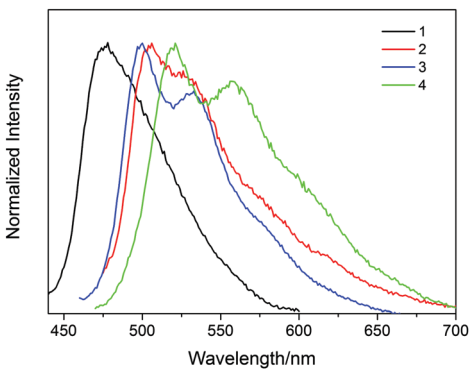

Fig. 4 Solid state emission spectra of **1–4** in powder.

Table 1 Spectroscopic and photophysical properties of the compound **1–4** (10^{-5} M) in DCM and powder

		λ_{abs}, N m^a	ε_{abs}, M cm^{-1}	λ_{em}, nm	$\Delta\nu_{em\text{-}abs}$ cm^{-1} ^{b}	Φ_F	τ_f, ns
1	CH_2Cl_2	378, 396(sh)	18 900	475	4199	0.21	4.14
	Powder			478		0.12	
2	CH_2Cl_2	402, 423(sh)	20 100	492	3315	0.25	4.19
	Powder			506, 526		0.06	
3	CH_2Cl_2	407, 430	22 300	437, 467	1842	0.39	1.93
	Powder			500, 533		0.10	
4	CH_2Cl_2	415, 437(sh)	19 000	492	2558	0.24	2.52
	Powder			521, 556		0.05	

^{a} sh = shoulder. ^{b} DFT calculation predict that the shoulder of absorption at the lower energy can be assigned to the S_0–S_1 transition (Fig. 6).

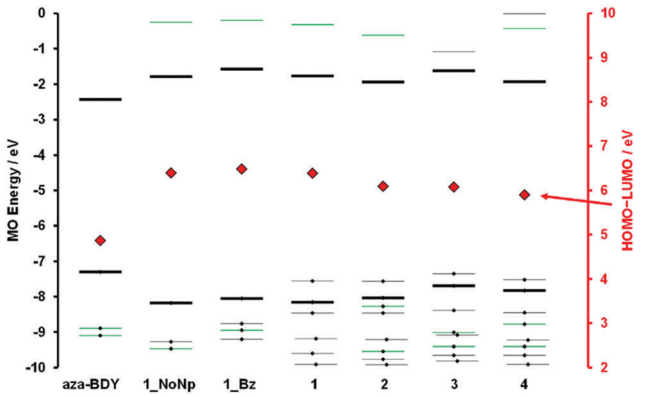

Fig. 5 MO energies for **1–4**, **aza-BDY**, **1_NoNp** and **1_Bz**. Small black diamonds denote occupied MOs. Thick black and green lines denote MOs derived from the HOMO and LUMO of **aza-BDY** or other π-MOs of the aza-BDY core. Thin black lines are used to highlight MOs that are introduced by peripheral fused benzene rings with σ-MOs offset to the right. The HOMO–LUMO gap values are plotted against a secondary axis.

The effect of fusion of a benzene ring at the 3,4-positions of the pyridine ring to form **3**, differs significantly from the fusion at the 2,3- and 4,5-positions to form **2** and **4**, because there is a nodal plane between the atoms at the 3,4-positions of the MOs derived from the HOMO and LUMO of aza-BODIPY (Fig. 7). This means that there is an antibonding interaction at the position of attachment of the fused benzene ring and hence a marked destabilization of the frontier π-MOs (Fig. 5), while there are bonding interactions in the context of **2** and **4**. The marked difference in the potential energy surfaces of the excited states is the most likely explanation for the presence of more well-resolved bands in the spectrum of **3** (Fig. 3). It is noteworthy that the angular nodal patterns of the HOMO and HOMO−1 are very similar (Fig. 7). This explains why the shoulder of intensity that is observed at low energy in the spectra of **1**, **2** and **4** becomes significantly more intense in the spectrum of **3**.

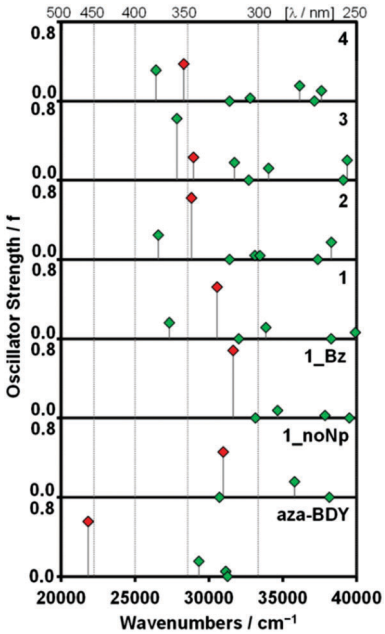

Fig. 6 TD-DFT calculations for **aza-BDY**, **1_NoNp**, **1_Bz** and **1–4**. Red diamonds are used to highlight the bands that arise primarily from the MOs derived from the HOMO and LUMO of the aza-BODIPY core (Fig. 5 and 7). The details of the calculations are provided as ESI.†

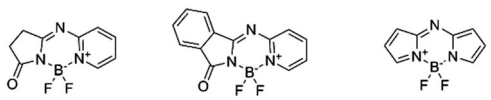

Scheme 3 Chemical structures of model complexes for structures equivalent to **1** with no peripheral fused rings (**1_NoNp**) or a benzene ring (**1_Bz**) and **aza-BDY**.

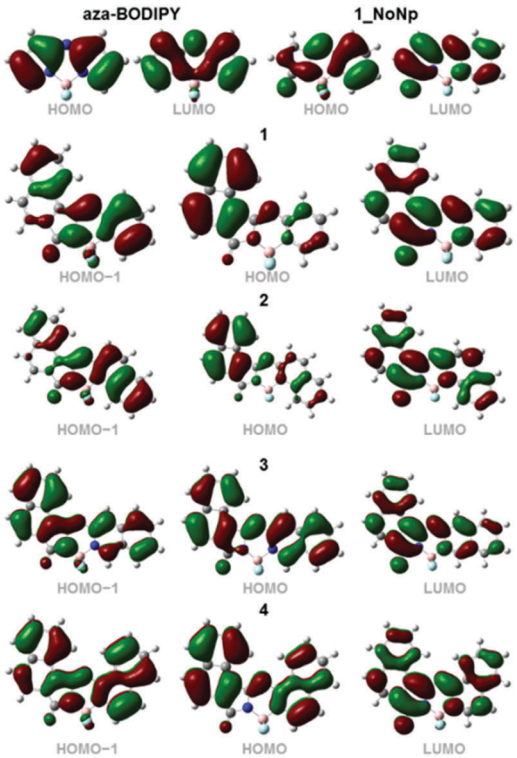

Fig. 7 Angular nodal patterns for **1–4**, and the **aza-BDY** and **1_NoNp** model compounds at an isosurface value of 0.02 a.u. Trends in the energies are shown in Fig. 5. The HOMO of **1–4** is largely localized on the peripheral naphthalene moiety, while the HOMO−1 is derived from the HOMO of the parent **aza-BDY** and **1_NoNp** model compounds.

Conclusion

Four aza boron-pyridyl-isoindoline analogues that differ in the position of fused benzene rings on the pyridyl moiety, have been synthesized through a facile two step reaction. Broad envelopes of intense vibrational bands are observed in the absorption spectra, since the peripheral fused rings introduce extra frontier π-MOs. Moderate Φ_F values are obtained in solution and effective emission intensity is observed in the solid state. Theoretical calculations predict that the impact of ring-fusion is highly dependent on the position at which the ring is introduced. Fusion at the 3,4-positions of the pyridyl moiety leads to a marked destabilization of the frontier π-MOs since there are stabilizing bonding interactions at the points of attachment, while there are bonding interactions in the context of fusion at the 2,3-positions and 4,5-positions.

Experimental section

Synthesis and characterisation

Synthesis of 1. A solution of 3-imino-1,2-benzoisoindoline-1-one **b** (330 mg, 1.0 mmol) and 2-aminopyridine (113 mg, 1.2 mmol) in ethanol (10 ml) was heated under reflux for 20 h. Ammonia was evolved. When the solution was cooled, a light yellow solid was precipitated. The crude product was dissolved in dry dichloromethane solution (100 ml) and treated with $BF_3{\cdot}OEt_2$ (2.2 ml) in the presence of triethylamine (2 ml) at room temperature for 1 h. The reaction was quenched by adding water, the organic layer was dried over $MgSO_4$, filtered, and evaporated to dryness. The crude product was purified by silica-gel flash column chromatography (75% hexane/ethyl acetate). Yield 155 mg (47%). UV-vis (CH_2Cl_2): λ_{max}, nm (ε) 378 (18 900 M cm^{-1}). ^1H NMR (400 MHz; CD_2Cl_2; Me_4Si): δ_H, ppm 9.40 (d, J = 8.4 Hz, 1H), 8.64 (d, J = 5.8 Hz, 1H), 8.22–8.15 (m, 2H), 7.98 (m, 2H), 7.86 (d, J = 8.3 Hz, 1H), 7.76 (m, 1H), 7.69 (m, 1H), 7.50 (t, J = 6.6 Hz, 1H). MS (HRMS-ESI): m/z 344.0780 (calcd for $[M + Na]^+$ 344.0780).

Compound 2 was obtained as yellow solid by following a procedure similar to that of 1. Yield 145 mg (39%). UV-vis (CH_2Cl_2): λ_{max}, nm (ε) 402 (20100 M cm^{-1}). ^1H NMR (400 MHz; CD_2Cl_2; Me_4Si): δ_H, ppm 9.43 (d, J = 8.5 Hz, 1H), 8.94 (d, J = 9.4 Hz, 1H), 8.50 (d, J = 8.8 Hz, 1H), 8.19 (d, J = 8.2 Hz, 1H), 8.00 (t, J = 8.6 Hz, 2H), 7.96–7.89 (m, 2H), 7.85 (d, J = 8.7 Hz, 1H), 7.81–7.77 (m, 1H), 7.70 (m, J = 7.2, 3.9 Hz, 2H). MS (HRMS-ESI): m/z 394.0934 (calcd for $[M + Na]^+$ 394. 0934).

Compound 3 was obtained as yellow solid by following a procedure similar to that of 1. Yield 126 mg (34%). UV-vis (CH_2Cl_2): λ_{max}, nm ($\log\varepsilon$) 407 (2.23). ^1H NMR (400 MHz; CD_2Cl_2; Me_4Si): δ_H, ppm 9.49 (d, J = 8.6 Hz, 2H), 8.25 (s, 1H), 8.19

(s, 1H), 8.14 (d, J = 8.0 Hz, 1H), 8.00 (m, 4H), 7.77 (s, 2H), 7.69 (d, J = 7.5 Hz, 1H). MS (HRMS-ESI): m/z 394.0937 (calcd for $[M + Na]^+$ 394.0934).

Compound 4 was obtained as yellow crystals by following a procedure similar to that of 1. Yield 116 mg (31%). UV-vis (CH_2Cl_2): λ_{max}, nm ($\log \varepsilon$) 415 (1.90). ^{1}H NMR (400 MHz; $CDCl_3$; Me_4Si): δ_H, ppm 9.54 (d, J = 8.4 Hz, 1H), 9.25 (d, J = 8.1 Hz, 1H), 8.38 (d, J = 6.5 Hz, 1H), 8.20 (d, J = 8.1 Hz, 1H), 8.00 (m, 5H), 7.91–7.87 (m, 1H), 7.74 (d, J = 9.6, 7.0 Hz, 2H). MS (HRMS-ESI): m/z 394.0939 (calcd for $[M + Na]^+$ 394. 0934).

The synthesis of d. A mixture of 1,2-naphthalenedicarnitrile (500 mg, 2.8 mmol) and *N*,*N*-diethylhydroxylamine (603 μL, 6.2 mmol) in freshly distilled dry $CHCl_3$ (10 mL) was placed in a round-bottom flask equipped with a magnetic stirrer and reflux condenser and refluxed for 4 h. The reaction mixture was cooled to room temperature, stirred for an additional 1 h, concentrated *in vacuo* and the residue chromatographed on a silica gel column (R_f = 0.2, hexane : ether = 1 : 1) to give **b** as a main product with yield of 38% and **d** as white powders with yield of 15%. For **d**: ^{1}H NMR (400 MHz; CD_2Cl_2; Me_4Si): δ_H, ppm 8.94 (d, J = 8.3 Hz, 1H), 8.21 (d, J = 8.3 Hz, 1H), 7.98 (d, J = 8.2 Hz, 1H), 7.87 (d, J = 8.3 Hz, 1H), 7.77–7.73 (m, 1H), 7.71–7.67 (m, 1H), 7.60 (s, 1H).

X-ray structure determination

The X-ray diffraction data were collected on a Bruker Smart Apex CCD diffractometer with graphite monochromated Mo Kα radiation (λ = 0.71073 Å) using the $\omega - 2\theta$ scan mode. The structure was solved by direct methods and refined on F^2 by full-matrix least-squares methods using SHELX-2000.[8] All calculations and molecular graphics were carried out by using the SHELX-2000 program package and Diamond 3.2.

1: $C_{17}H_{10}BF_2N_3O$; a block-like crystal of the approximate dimensions 0.30 × 0.20 × 0.20 mm^3 was measured. Orthorhombic, space group $Pca2_1$, a = 18.945 (1) Å, b = 4.954 (3) Å, c = 15.200 (9) Å, α = 90, β = 90, γ = 90, V = 1426.5 (1) Å^3, Z = 4, F(000) = 656.0, ρ = 1.490 Mg m^{-3}, R_1 = 0.0654, wR_2 = 0.1848, GOF = 1.012, residual electron density between 0.241 and −0.308 e Å^{-3}.

d: $C_{12}H_7NO_2$: A block-like crystal of the approximate dimensions 0.25 × 0.20 × 0.20 mm^3 was measured. Monoclinic, space group $P2_1/c$, a = 3.8800 (1) Å, b = 11.779 (4) Å, c = 19.292 (6) Å, α = 90, β = 90.211(8), γ = 90, V = 881.7(5) Å^3, Z = 4, F(000) = 408, ρ = 1.486 Mg m^{-3}, R_1 = 0.0531, wR_2 = 0.1578, GOF = 0.900, residual electron density between 0.182 and −0.181 e Å^{-3}.

CCDC 1503936† for **1** and 1503937† for **d** containing the supplementary crystallographic data for this paper.

Spectroscopic measurements

UV-visible absorption spectra were recorded on a Shimadzu 3000 spectrophotometer. The fluorescence lifetimes and fluorescence spectra were measured on Horiba Jobin Yvon Fluorolog-3. Absorption and emission measurements were carried out in 1 × 1 cm quartz cuvettes. Emission spectra and the absolute quantum yields in the solid state were measured in Horiba Jobin Yvon Fluorolog-3 spectrofluorimeter with an integrating sphere. The temperature was kept constant at (298 ± 2) K for all measurements. Dilute solutions with absorbance values of less than 0.05 at the excitation wavelength were used for the measurement of fluorescence quantum yields. 9,10-Diphenylanthracene was used as the standard (Φ_F = 0.90 in cyclohexane).[9] The quantum yield, Φ, was calculated using eqn (1):

$$\Phi_{sample} = \Phi_{std}\left[\frac{I_{sample}}{I_{std}}\right]\left[\frac{A_{std}}{A_{sample}}\right]\left[\frac{n_{sample}}{n_{std}}\right]^2 \quad (1)$$

where the sample and std subscripts denote the sample and standard, respectively, I is the integrated emission intensity, A stands for the absorbance, and n is refractive index.

Density functional theory calculations

The Gaussian09 software package[10] was used to carry out geometry optimizations for **1–4**, aza-BODIPY (**aza-BDY**) and two model complexes equivalent to **1** with no peripheral fused rings (**1_NoNp**) or a benzene ring (**1_Bz**) (Scheme 3) by using the B3LYP functional with 6-31G(d) basis sets. The CAM-B3LYP functional was used to carry out TD-DFT calculations, since it provides a long-range correction that makes it more suitable for use with compounds that have excited states with significant charge transfer character.[11] The polarized continuum model (PCM) was used to introduce a CH_2Cl_2 solvation environment.

Acknowledgements

Financial support was provided by the National Natural Science Foundation of China (no. 21471042) to LH, the National Research Foundation of South Africa through a CSUR grant (uid: 93627) to JM.

References

1 (*a*) D. Kumaresan, R. P. Thummel, T. Bura, G. Ulrich and R. Ziessel, *Chem. – Eur. J.*, 2009, **15**, 6335–6339; (*b*) J. Fan, M. Hu, P. Zhan and X. Peng, *Chem. Soc. Rev.*, 2013, **42**, 29–43; (*c*) J. Zhao, W. Wu, J. Sun and S. Guo, *Chem. Soc. Rev.*, 2013, **42**, 5323–5351; (*d*) D. Li, H. Zhang and Y. Wang, *Chem. Soc. Rev.*, 2013, **42**, 8416–8433; (*e*) Z. Liu, W. He and Z. Guo, *Chem. Soc. Rev.*, 2013, **42**, 1568–1600.

2 (*a*) H. Lu, J. Mack, Y. Yang and Z. Shen, *Chem. Soc. Rev.*, 2014, **43**, 4778–4823; (*b*) G. Ulrich, R. Ziessel and A. Harriman, *Angew. Chem., Int. Ed.*, 2008, **47**, 1184–1201; (*c*) N. Boens, V. Leen and W. Dehaen, *Chem. Soc. Rev.*, 2012, **41**, 1130–1172; (*d*) A. Loudet and K. Burgess, *Chem. Rev.*, 2007, **107**, 4891–4932.

3 (*a*) H. Lu, Q. Wang, L. Gai, Z. Li, Y. Deng, X. Xiao, G. Lai and Z. Shen, *Chem. – Eur. J.*, 2012, **18**, 7852–7861; (*b*) Q. Liu, X. Wang, H. Yan, Y. Wu, Z. Li, S. Gong, P. Liu and Z. Liu, *J. Mater. Chem. C*, 2015, **3**, 2953–2959; (*c*) X. Wang, Q. Liu, H. Yan, Z. Liu, M. Yao, Q. Zhang, S. Gong and W. He, *Chem. Commun.*, 2015, **51**, 7497–7500; (*d*) C. Yu, E. Hao, T. Li, J. Wang, W. Sheng, Y. Wei, X. Mu and L. Jiao, *Dalton Trans.*, 2015, **44**, 13897–13905; (*e*) S. Shimizu, A. Murayama,

T. Haruyama, T. Lino, S. Mori, H. Furuta and N. Kobayashi, *Chem. – Eur. J.*, 2015, **21**, 12996–13003; (*f*) L. Gai, H. Lu, B. Zou, G. Lai, Z. Shen and Z. Li, *RSC Adv.*, 2012, **2**, 8840–8846; (*g*) X. Wang, H. Liu, J. Cui, Y. Wu, H. Lu, J. Lu, Z. Liu and W. He, *New J. Chem.*, 2014, **38**, 1277–1284; (*h*) N. Gao, C. Cheng, C. Yu, E. Hao, S. Wang, J. Wang, Y. Wei, X. Mu and L. Jiao, *Dalton Trans.*, 2014, **43**, 7121–7127.

4 H. Liu, H. Lu, Z. Zhou, S. Shimizu, Z. Li, N. Kobayashi and Z. Shen, *Chem. Commun.*, 2015, **51**, 1713–1716.

5 (*a*) H. Liu, H. Lu, J. Xu, Z. Liu, Z. Li, J. Mack and Z. Shen, *Chem. Commun.*, 2014, **50**, 1074–1076; (*b*) Y. Wu, H. Lu, S. Wang, Z. Li and Z. Shen, *J. Mater. Chem. C*, 2015, **3**, 12281–12289; (*c*) H. Liu, H. Lu, F. Wu, Z. Li, N. Kobayashi and Z. Shen, *Org. Biomol. Chem.*, 2014, **12**, 8223–8229; (*d*) Y. Wu, S. Wang, Z. Li, Z. Shen and H. Lu, *J. Mater. Chem. C*, 2016, **4**, 4668–4674; (*e*) H. Liu, Y. Wu, Z. Li and H. Lu, *J. Porphyrins Phthalocyanines*, 2014, **18**, 679–685.

6 K. V. Luzyanin, V. Yu. Kukushkin, M. N. Kopylovich, A. A. Nazarov, M. Galanski and A. J. L. Pombeiro, *Adv. Synth. Catal.*, 2008, **350**, 135–142.

7 J. Killoran, L. Allen, J. Gallagher, W. Gallagher and D. F. O'Shea, *Chem. Commun.*, 2002, 1862–1863.

8 G. M. Sheldrick, *Acta Crystallogr., Sect. D: Biol. Crystallogr.*, 2008, **64**, 112–122.

9 S. Hamai and F. Hirayama, *J. Phys. Chem.*, 1983, **87**, 83–89.

10 M. J. Frisch, G. W. Trucks, H. B. Schlegel, G. E. Scuseria, M. A. Robb, J. R. Cheeseman, G. Scalmani, V. Barone, B. Mennucci, G. A. Petersson, H. Nakatsuji, M. Caricato, X. Li, H. P. Hratchian, A. F. Izmaylov, J. Bloino, G. Zheng, J. L. Sonnenberg, M. Hada, M. Ehara, K. Toyota, R. Fukuda, J. Hasegawa, M. Ishida, T. Nakajima, Y. Honda, O. Kitao, H. Nakai, T. Vreven, J. A. Montgomery, J. E. Peralta, F. Ogliaro, M. Bearpark, J. J. Heyd, E. Brothers, K. N. Kudin, V. N. Staroverov, R. Kobayashi, J. Normand, K. Raghavachari, A. Rendell, J. C. Burant, S. S. Iyengar, J. Tomasi, M. Cossi, N. Rega, J. M. Millam, M. Klene, J. E. Knox, J. B. Cross, V. Bakken, C. Adamo, J. Jaramillo, R. Gomperts, R. E. Stratmann, O. Yazyev, A. J. Austin, R. Cammi, C. Pomelli, J. W. Ochterski, R. L. Martin, K. Morokuma, V. G. Zakrzewski, G. A. Voth, P. Salvador, J. J. Dannenberg, S. Dapprich, A. D. Daniels, Ö. Farkas, J. B. Foresman, J. V. Ortiz, J. Cioslowski and D. J. Fox, *Gaussian 09, Revision D.01*, Gaussian, Inc., Wallingford CT, 2009.

11 (*a*) Z. L. Cai, M. J. Crossley, J. R. Reimers, R. Kobayashi and R. D. Amos, *J. Phys. Chem. B*, 2006, **110**, 15624–15632; (*b*) J. Mack, M. Wildervanck and T. Nyokong, *Turk. J. Chem.*, 2014, **38**, 1013–1026.